Nuclear-Magnetic-Resonance Studies of Er^{167} in Erbium Iron Garnet

R. L. Streever and P. J. Caplan
United States Army Electronics Technology and Devices Laboratory, Fort Monmouth, New Jersey 07703
(Received 16 March 1973)

The nuclear magnetic resonance of Er^{167} in erbium iron garnet (ErIG) has been studied at 4.2 °K using both single crystals and polycrystalline powders. The zero-field spectrum obtained with the powder samples shows the existence of two types of rare-earth sites that would be expected when the magnetization is along a ⟨100⟩ direction. The two types of sites are found to have hyperfine fields of about 5.74×10^6 and 2.87×10^6 G, while the absolute magnitudes of the quadrupole coupling constants, $P = eQV_{zz}/4I(2I-1)h$, for the two sites are found to be 17 and 1 MHz, respectively. With an external field of a few kilogauss applied along a ⟨100⟩ direction of the single crystal, the Er^{167} spectrum is found to be similar to the zero-field powder spectrum, in agreement with the fact that ⟨100⟩ is an easy direction of magnetization in ErIG. With the external field oriented along a ⟨111⟩ direction of the crystal, the observed spectrum is found to be quite different from the ⟨100⟩ spectrum and more difficult to interpret in detail. Hyperfine fields and quadrupole coupling constants are discussed and compared with those expected from other studies. Nuclear relaxation times at the various sites have been measured and interpreted in terms of a relaxation mechanism involving the slow relaxation of the rare-earth ion.

I. INTRODUCTION

Nuclear-magnetic-resonance (NMR) studies in the rare-earth iron garnets are of interest because they can give very detailed information concerning the magnetic properties and hyperfine interactions of the magnetic ions. Erbium iron garnet (ErIG) is of particular interest because magnetic studies[1] and optical studies[2] have shown that while both ⟨111⟩ and ⟨100⟩ directions are relatively easy directions of magnetization at 4.2 °K, a ⟨100⟩ direction is easiest. This was confirmed in a previous communication,[3] where we reported briefly on the zero-field NMR of both Er^{167} and Fe^{57} in polycrystalline ErIG. In the present study we have extended our previous zero-field studies. By using single crystals and externally applied fields we have been able to study the Er^{167} NMR spectrum with the magnetization aligned along both ⟨111⟩ and ⟨100⟩ directions. From these studies and the results of Mössbauer studies,[4] which have also been carried out on ErIG, we have been able to obtain detailed information concerning the magnetic hyperfine fields and electric field gradients associated with the Er^{+3} ions. We have also carried out measurements of the Er^{167} relaxation times. From these studies we have been able to obtain information concerning the details of the Er^{+3} relaxation in ErIG.

A brief discussion of the hyperfine parameters is given in Sec. II. Experimental techniques are discussed and results of the spectral NMR studies are given in Sec. III. A discussion of the Er hyperfine field parameters is given in Sec. IV. The relaxation time studies are discussed in Sec. V.

II. HYPERFINE INTERACTIONS

A. Anisotropic Hyperfine Field

Hyperfine fields at rare-earth nuclei have been discussed by several authors. The major contribution to the internal field comes from the $4f$ electrons and can be written

$$H_{\text{int}} = 2\mu_B N \langle r^{-3} \rangle_{\text{eff}} \langle J_z \rangle. \tag{1}$$

A similar expression can be written for the magnetic moments,

$$\langle \mu_z \rangle = \lambda \mu_B \langle J_z \rangle. \tag{2}$$

The factors N and λ have been tabulated[5,6] for the various rare-earth ions. For Er^{+3}, $N = 0.78$ and $\lambda = \frac{6}{5}$. From (1) and (2) there should be a good proportionality between the ground-state magnetic moment and hyperfine field.

The rare-earth ions in the iron garnets reside at sites which are known to possess a local orthorhombic symmetry. The local orthorhombic axes of these sites take on six orientations with respect to the crystal axes, resulting in general in six magnetically inequivalent rare-earth sites.[7] For one of the sites the orthorhombic z axis can be chosen to lie along a cubic ⟨001⟩ direction, while the x and y axes lie along ⟨110⟩ and ⟨1$\bar{1}$0⟩ directions. The other orthorhombic sites can be generated by taking the orthorhombic axes to be along equivalent directions.

For the case where the Fe magnetization $\vec{M}_{Fe}$ lies along a cubic ⟨100⟩ direction, two types of rare-earth sites, c_1 and c_2, arise with relative site populations of 2:4. If we let (n_x, n_y, n_z) be the direction cosines between $\vec{M}_{Fe}$ and the orthorhombic axes, then for sites c_1 the direction co-

sines are (0, 0, 1), while for sites c_2 they are $(\sqrt{\frac{1}{2}}, \sqrt{\frac{1}{2}}, 0)$. For the case where the Fe magnetization lies along a cubic ⟨111⟩ direction, two types of rare-earth sites, c_1' and c_2', arise with relative site populations of 3:3, and with direction cosines $(\sqrt{\frac{2}{3}}, 0, \sqrt{\frac{1}{3}})$ and $(0, \sqrt{\frac{2}{3}}, \sqrt{\frac{1}{3}})$.

For the case of a Kramers doublet, explicit expressions for the ground-state magnetic moments (in zero field) can be obtained.[7]

B. Electric Field Gradient

For an arbitrary orientation of the rare-earth moment one can define an effective quadrupole interaction parameter as

$$P_{eff} = \frac{eQV_{eff}}{4I(2I-1)h} . \tag{3}$$

V_{eff}, the effective electric field gradient, can be written as the sum of a $4f$ contribution V_{4f} and a contribution from the external lattice charges,

$$V_{eff} = V'_{4f} + V'_{lat}. \tag{4}$$

The electric field gradient arising from the $4f$ electrons can be written, assuming J to be a good quantum number, as

$$V'_{4f} = -e\alpha\langle r^{-3}\rangle_{eff}\langle 3J_{z'}^2 - J(J+1)\rangle (1-R). \tag{5}$$

In (4) and (5) the prime denotes the quantities must be evaluated for an arbitrary orientation of the rare-earth moment along the direction z'. For the Er^{+3} ion the matrix element[5] α is $\frac{4}{1575}$.

The lattice contribution can be written

$$V'_{lat} = \tfrac{1}{2}V_{zz}[3h_z^2 - 1 + \eta(h_x^2 - h_y^2)]. \tag{6}$$

In (6), V_{zz} is the electric field gradient along the orthorhombic z axis (which coincides with a crystal ⟨100⟩ axis) and h_x, h_y, and h_z are the direction cosines between z' and the orthorhombic axes.

We can express V_{zz} in terms of the crystal field parameter $V_2^0 \equiv A_2^0\langle r^2\rangle$ as

$$V_{zz} = \frac{-4V_2^0(1-\gamma_\infty)}{(1-\sigma_2)e\langle r^2\rangle} . \tag{7}$$

In (7), σ_2 and γ_∞ are shielding parameters.

III. EXPERIMENTAL

A. Equipment and Measuring Technique

The spin-echo equipment employed a high-power pulsed oscillator (Applied Microwave Lab PG1K), receivers, and calibration oscillators to cover the required frequency range. For the resonant element two types of cavities were used, the rectangular quarter-wave cavity described previously,[8] and a cylindrical quarter-wave coaxial cavity. The cylindrical cavity, which was tuned by varying the length of the reentrant stub, had a higher Q than the rectangular cavity and could be made to operate at frequencies of up to nearly 2000 MHz. Double-stub tuners were used in both input and output lines of the cavity.

Both polycrystalline and single-crystal samples of ErIG were studied. The polycrystalline sample consisted of about 15 g of finely divided powder which was sealed in a glass tube. The single-crystal sample, which weighed about 10 g, was roughly spherical in shape. It was mounted so that it could be rotated about a ⟨110⟩ axis which was parallel to the rf field and perpendicular to the external dc field. All measurements were carried out at 4.2 °K with an exposed-tip Dewar vessel, the tip of which fitted into the cavity. An external dc field H_{ext} of several kilogauss was used in the single-crystal studies to drive out domain walls and orient the magnetization along one of the easy directions. Spectral studies were made for a given crystal orientation by plotting spin-echo amplitudes as a function of frequency.

In addition to the spectral measurements of spin-echo intensity, relaxation time studies were carried out and will be discussed more fully in Sec. V.

B. Results

The zero-field Er^{167} spectrum obtained with the powder sample at 4.2 °K is shown in Fig. 1. Since the easy direction of magnetization for ErIG is ⟨100⟩, we expect the spectrum obtained with the crystal oriented so that $\vec{H}_{ext}$ is along ⟨100⟩ to be the same as the zero-field spectrum. This was found to be the case. The spectrum obtained with $\vec{H}_{ext}$ along ⟨100⟩ was basically the same as the zero-field spectrum except that the various lines were found to be shifted from their zero-field frequencies as shown in Table I.

The direct effect of the external field on the nuclear moment would only be expected to shift the frequency by about 1 MHz. The larger observed shifts may indicate slightly field-dependent magnetic moments. The lines between 350 and 375 MHz were not all observed with an external field, probably being too weak. The line at 346 MHz shifted to a slightly lower frequency at 4.5 kG. This is a contrast to the remaining lines, which shifted to higher frequencies.

The spectrum observed at 4.2 °K with an applied

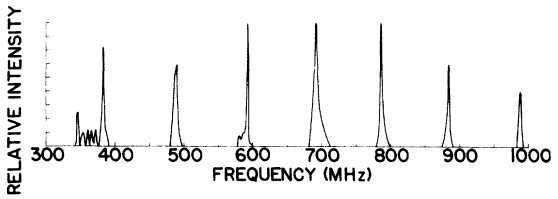

FIG. 1. ErIG zero-field spectrum at 4.2 °K.

TABLE I. Resonance frequencies for the various ⟨100⟩ lines in zero field and for applied fields of 4.5 and 8.0 kG.

Field (kG)	Line frequency (MHz)							
0	346	384	489	590	692	791	899	988
4.5	343	386	491	593	693	795	893	995
8.0	···	386	495	596	697	796	···	···

field of 8 kG along a ⟨111⟩ direction of the crystal is shown in Fig. 2.

IV. DISCUSSION

A. Hyperfine Field Parameters

Since for Er^{167} $I=\frac{7}{2}$, we expect the NMR of each site to show the usual seven-line quadrupole splitting pattern, with a splitting between lines given by Δ, where $\Delta = |6P_{eff}|$ and P_{eff} was defined previously.

Hüfner *et al.*[4] have studied the hyperfine structure of Er^{166} in ErIG using the Mössbauer technique. They fitted their zero-field spectrum assuming two types of rare-earth sites with relative site populations of 3:3, corresponding to $\vec{M}_{Fe}$ being along ⟨111⟩. Since in zero field $\vec{M}_{Fe}$ lies along ⟨100⟩, their spectrum should have been fitted with a 2:4 relative site population. In any case, we might expect the Mössbauer hyperfine data to be approximately correct. The Mössbauer results indicate hyperfine fields at the two types of sites of $(5.55\pm0.5)\times10^6$ and $(3.90\pm0.2)\times10^6$ G with quadrupole coupling constants P of $(1.75\pm0.35)\times10^{-7}$ and $(0.25\pm0.35)\times10^{-7}$ eV, respectively.

Now consider the Er^{167} NMR spectrum of Fig. 1. Taking the nuclear moment of Er^{167} to be $-0.56\mu_N$[9] we expect (from the Mössbauer results) to observe two seven-line patterns centered at 670 ± 60 and 470 ± 24 MHz. Taking Q of the Er^{166} excited state to be -2.1 ± 0.2 b[10] and Q of Er^{167} to be $+3.0\pm0.4$ b,[9] we expect a splitting Δ between adjacent lines of 104 and 15 MHz for the respective sites. If we take the line at 692 MHz to be the center of one seven-line pattern corresponding to the site with the higher hyperfine field we see that the corresponding splitting between adjacent lines, which is about 100 MHz, would be in good agreement with the Mössbauer result. The group of lines extending from 346 to 375 MHz would then have to be attributed to the other site.

Khoi[11] has also studied the zero-field Er^{166} NMR in ErIG at 4.2 °K. He finds lines at nearly the same frequencies as we do but did not observe the lines from 346–375 MHz. He concludes rather that the lines from the site with the lower hyperfine field coincide with the line at 489 MHz. Although this interpretation would agree better with the Mössbauer results, it could not explain the lines from 346–375 MHz. Furthermore, with an applied field, all the lines including the one at 489 MHz had a width of about 2 MHz. Consequently, it seems likely that the lines between 346 and 375 MHz do belong to the site with the lower hyperfine field.

Using (1) and (2) and taking as was done in Ref. 4 $\langle r^{-3}\rangle_{eff}=72\times10^{24}$ cm^{-3}, we can calculate effective magnetic moments at the two ⟨100⟩ sites of about $6.6\mu_B$ and $3.4\mu_B$. These magnetic moments can be compared with magnetic moments of $6.9\mu_B$ and $4.8\mu_B$ obtained for the two types of ⟨100⟩ sites from optical studies.[2] Because of the numerous factors effecting the intensities it would be difficult from the NMR to say which group of lines correspond to site c_1. The optical studies, however, indicate that the ⟨100⟩ site with the larger moment corresponds to site c_1.

For the case of $\vec{M}_{Fe}$ along ⟨111⟩ the optical studies give moments of $5.3\mu_B$ and $4.7\mu_B$. From this we would expect the ⟨111⟩ hyperfine fields to be about 4.6×10^6 and 4.1×10^6 G, corresponding to frequencies of 556 and 499 MHz. A detailed interpretation of the ⟨111⟩ spectrum of Fig. 2 is difficult. One site appears to have a line splitting of about 40 MHz. The center of gravity of the whole distribution is in approximate agreement with what one would expect from the optical moments.

From the experimentally observed ground-state moments one should be able to derive a set of principle moments (μ_x, μ_y, and μ_z) for the orthorhombic sites. The expressions[7] for the ground-state moments involve rare-earth–iron exchange parameters which are not known precisely. Taking $\mu_z=6.9\mu_B$, and moments of $4.3\mu_B$ and $5.2\mu_B$ corresponding to the other two orthorhombic axes, would give approximate agreement with the optical moments provided reasonable exchange parameters were assumed.

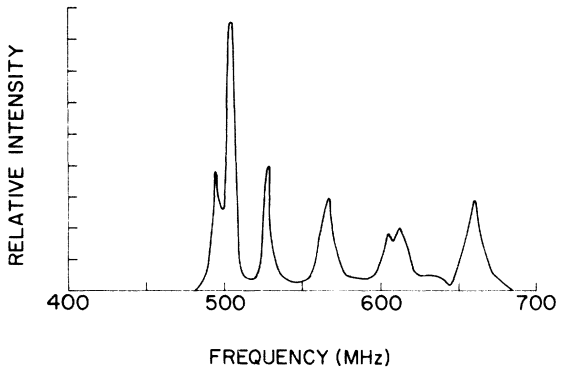

FIG. 2. ErIG spectrum with an external field of 8 kG along the ⟨111⟩ direction at 4.2 °K.

B. Electric Field Gradients

In this section we will discuss contributions to the electric field gradients. From (5) one can calculate a free-ion value for P_{4f} of about -18 MHz. Because of the crystal fields, P_{4f} will be reduced from the free-ion value. Khoi has calculated P_{4f} for the two $\langle 100\rangle$ sites c_1 and c_2 to be -9.7 and -2.7 MHz, respectively. Taking $P_{zz\,\mathrm{lat}}$ to be about -7 MHz and using (6) would give lattice contributions to P at the two $\langle 100\rangle$ sites of -7 and 3.5 MHz. The net P_{eff} would then be about -17 MHz for site c_1 and $+1$ MHz for site c_2. The values of P_{eff} would be in agreement with NMR studies and the sign of P_{eff} would be consistent with the Mössbauer studies

For the $\langle 111\rangle$ sites the $4f$ contribution to P can be estimated to be about -4 MHz. Assuming $|\eta| = 1$ and using (6) would give lattice contributions for the $\langle 111\rangle$ sites of ± 2 MHz. The net P_{eff} for the two sites would then be -6 and -2 MHz. These values of P would correspond to splittings between adjacent lines of 36 and 12 MHz and would be consistent with an observed splitting for one site of 40 MHz.

Using (3) and (7) one can calculate V_2^0 from the value of $P_{zz\,\mathrm{lat}}$. Taking for $(1-\gamma_\infty)/(1-\sigma_2)$ a value of 280 (as was done in Ref. 8) and for $\langle r^2\rangle$ a value[12] of 0.19×10^{-16} cm^2, we obtain $V_2^0 = 113$ cm^{-1}. It is of interest to compare this with values of V_2^0 obtained from optical studies.[13] We must recall that our value of V_2^0 is referred to the orthorhombic axis which lies along a $\langle 100\rangle$ direction. The crystal field parameters for ErGaG referred to the same axis would be $V_2^0 = 62$ cm^{-1} and $\eta = V_2^2/V_2^0 = \pm\frac{2}{3}$. We see that the value of V_2^0 obtained from the quadrupole splitting is about a factor of 2 larger than that obtained from the optical studies. Whether this reflects a real difference in the value of V_2^0 for ErIG and ErGaG or simply reflects some uncertainty in the shielding parameters is not clear.

V. RELAXATION TIMES

A. Preliminary Discussion

The Er^{167} relaxation is complicated by the quadrupolar splitting. The relaxation of a quadrupolar-split spectrum has been discussed by several authors.[14,15] We will assume a model in which the Er^{167} nuclei are relaxed by a fluctuating component of the hyperfine field perpendicular to the quantization direction. For this case the relaxation will be magnetic dipolar and the transition probability for transitions between adjacent nuclear levels will be given by an expression of the form

$$W_{m\pm1\to m} = W(I\mp m)\,(I\pm m+1). \tag{8}$$

In Sec. V C we will develop a detailed expression for W. From general considerations we would expect W to depend on the square of the hyperfine field and also on a correlation factor given by $\tau(1+\omega^2\tau^2)^{-1}$, where τ is the correlation time associated with the fluctuating field and $\omega/2\pi$ is the nuclear-resonance frequency. We will show in Sec. V C that $\omega\tau \ll 1$. For this case W depends on the frequency of the central transition through the hyperfine field but is the same for each transition.

The case where W can be considered to be the same for each transition has been discussed in Ref. 14.

Following Ref. 14 one can define population differences a_m between various levels by the relation $a_m(t) = n_m(t) - n_{m-1}(t)$, where the quantity $n_m(t)$ is the departure of the fractional relative population of the mth state from its thermal equilibrium value. The population differences are given as a sum of exponentials:

$$a_m(t) = \sum_j a_{mj} e^{-\lambda_j t}. \tag{9}$$

For a spin-$\frac{7}{2}$ system $\lambda_j/W = 2, 6, 12, 20, 32, 42$, and 56. The a_{mj} depend on the particular transition and on the initial conditions. In general, the relaxation will be nonexponential and only at long times will it proceed with the characteristic time $T_1 = 1/2W$ that would be expected for a spin-$\frac{1}{2}$ system.

1. Stimulated Echo Method

In the absence of spin diffusion the stimulated echo decay measures the longitudinal relaxation. The initial conditions correspond to the inversion of a single transition [$a_m(0) = -2\beta$, $a_{m-1}(0) = a_{m+1}(0) = \beta$, all other $a_m = 0$]. For $I = \frac{5}{2}$ explicit expressions for the decay curves have been given in Ref. 14. Corresponding expressions for $I = \frac{7}{2}$ can be easily obtained by using the matrices given in Ref. 15. Stimulated echo decay curves corresponding to excitation of the various transitions are plotted in Fig. 3. Note that at long times the decay proceeds at a rate $T_1 = 1/2W$ that would be expected for a spin-$\frac{1}{2}$ system.

2. Saturation Method

With the saturation method one monitors the recovery of the magnetization following a series of closely spaced saturating pulses. Two cases have been discussed by Narath.[15] With a relatively short saturating comb one assumes that a given transition is saturated but that the populations of the other levels do not have time to adjust accordingly. In this case (case C of Ref. 15) the magnetization recovery $[1 - m(t)/m(\infty)]$ is the same as the stimulated echo decay. With longer saturating combs (case B of Ref. 15) one assumes that a given transition is saturated and that the other levels have time to adjust accordingly. For this case the initial conditions are just $a_m(0) = \beta$, all others zero. The recovery curves are nonexponential as for the short

TABLE II. Relaxation times for the lines corresponding to $\vec{M}_{Fe}$ along ⟨100⟩ in zero field and for $H_{ext} = 4.5$ kG.

Site	Line frequency (MHz) $H_{ext}=0$ (powder)	Line frequency (MHz) $H_{ext}=4.5$ kG (crystal)	T_s(initial) (μsec) $H_{ext}=0$ (powder)	T_s(initial) (μsec) $H_{ext}=4.5$ kG (crystal)	T_2(initial) (μsec) $H_{ext}=0$ (powder)	T_2(initial) (μsec) $H_{ext}=4.5$ kG (crystal)
	988	995	220	300	24	•••
	889	893	130	150	24	•••
	791	795	95	125	20	•••
c_1	692	693	65	120	20	37
	590	593	115	130	20	43
	489	491	130	155	32	42
	384	386	170	330	26	50
c_2	346	343	•••	200	•••	143

saturating comb, but a relatively larger amount of long-time component is obtained.

B. Er^{167} Relaxation Times

1. Relaxation Times with the Magnetization along ⟨100⟩

Relaxation time studies were carried out for the various ⟨100⟩ lines. Studies were made both in zero field using the powder sample and with an applied field of 4.5 kG using the single crystal. Relaxation times T_s (initial) obtained from the initial slopes of the stimulated echo decay curves are listed in Table II along with values of T_2 obtained from the echo decay. The stimulated echo decays were nearly independent of the exciting pulse separation, indicating that spin diffusion was small. We see that for site c_1 the relaxation times are nearly the same for corresponding lines on either side of the central $\frac{1}{2}\leftrightarrow\frac{1}{2}$ transition. This is in agreement with the calculated relaxation curves. By fitting the initial stimulated echo decays to the curves of Fig. 3 we obtain a T_1 for site c_1 of about 2.8 msec for $H_{ext} = 4.5$ kG, and about 2 msec in zero field. We also obtained T_1 for this site by the saturation method from the slope at long times. At 4.5 kG we obtained a T_1 of about 6 msec. The discrepancy between the two methods may be due in part to the effects of spin diffusion.

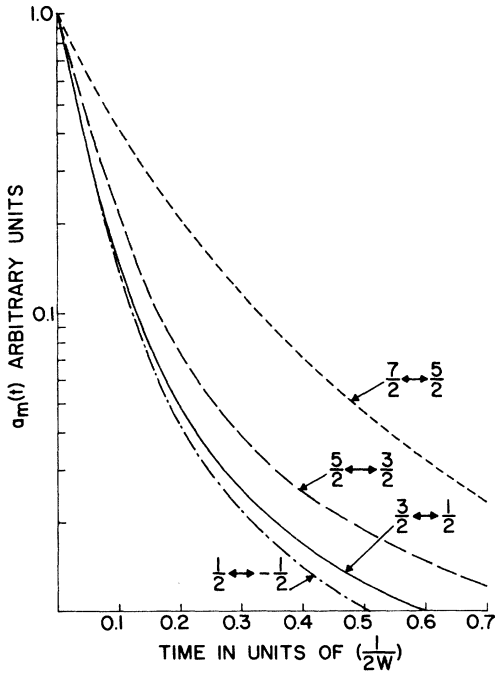

FIG. 3. Stimulated echo decay curves expected for the various transitions of an $I=\frac{7}{2}$ system. Decay curves for transitions on either side of the central one are the same.

For site c_2, using the line at 346 MHz, we obtained a T_1 from the saturation method of about 5 msec at 4.5 kG. This can be compared with a T_1 of about 4.5 msec that would be estimated from the initial stimulated echo decay.

For the central transition of site c_1 we also obtained with the single crystal the field dependence of T_s (initial) and T_2. This is plotted in Fig. 4.

2. Relaxation Times with the Magnetization along ⟨111⟩

Less detailed relaxation time studies were made for the ⟨111⟩ lines because of the more complex spectra. With an applied field of 5.6 kG T_2 varied between about 6 and 9 μsec. T_s(initial) was about 44 μsec for the line at 660 MHz, while for the other ⟨111⟩ lines T_s was of the order of T_2. This suggests that the line at 660 MHz may be from a different ⟨111⟩ site than the other lines.

T_1 obtained by saturating the line at around 500 MHz was about 50 μsec (with an applied field of 4.5 kG), while T_2 was about 9 μsec for the same

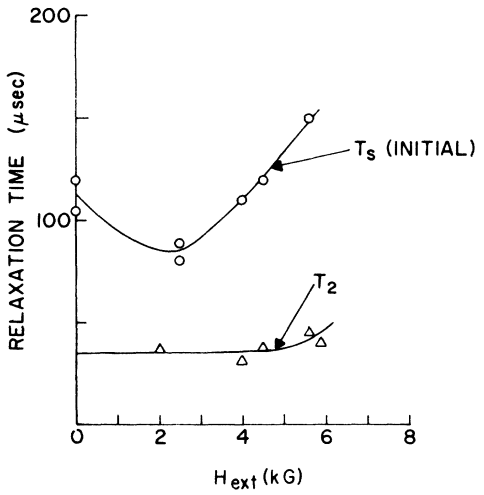

FIG. 4. Field dependence of T_s (initial) and T_2 for the central transition of site c_1.

line. No saturation study of the line at 660 MHz was carried out, but from T_s(initial) we can estimate T_1 to be of the order of 1 msec.

Estimated values of T_1 for different sites for both ⟨100⟩ and ⟨111⟩ orientations are summarized in Table III.

C. DISCUSSION

The Fe^{57} relaxation in rare-earth-doped YIG has been discussed in detail by Hartmann-Boutron[16] and involves the indirect coupling of the Fe^{57} nucleus to the rare-earth ion. The Fe^{57} relaxation in Yb-doped YIG has been shown[17] to be in agreement with the predictions of a slow-relaxation theory[16,18] for the rare-earth ion. In the slow-relaxation theory, because of the anisotropic rare-earth–iron exchange interaction, the slowly relaxing rare-earth ion can create a fluctuating transverse field which acts on the iron spin. This transverse field excites spin waves which eventually relax the Fe^{57} nuclei.

Consider now the rare-earth–nuclear relaxation. There should be a related direct interaction in which the relaxing rare-earth ion creates a transverse fluctuating hyperfine field at the nucleus of the same atom. The calculation of the rare-earth relaxation time from such an interaction can be carried through by analogy with the corresponding Fe^{57} relaxation.

By analogy with Eq. (1) of Ref. 16 one can express the direct interaction between the rare earth and nuclear spins as

$$\mathcal{H} = \sum_{\alpha a} A^{\alpha a} I^a J^\alpha . \tag{10}$$

In (10), $\vec{I}$ and $\vec{J}$ are the nuclear and rare-earth spin operators, and the $A^{\alpha a}$ describe the anisotropic hyperfine interaction. The fluctuating effective field at the rare-earth nucleus can then be written as[16]

$$H^{\pm} = H^x \pm iH^y = \frac{1}{\hbar\gamma_n} \sum_\alpha (A^{\alpha x} \pm iA^{\alpha y}) \delta J^\alpha . \tag{11}$$

Using (11) to carry through the calculation of T_1 [as far as Eq. (5) of Ref. 16] one finds the resulting expression the same as for the Fe^{57} case, except that terms involving the indirect Fe^{57} coupling via spin waves are absent and the quantities involving the anisotropic Fe–rare-earth interaction must be replaced by the corresponding quantities involving the anisotropic hyperfine interaction. Making these changes in Eq. (1) of Ref. 17 one obtains, for T_1,

$$\frac{1}{T_1} = F[\gamma H_{\rm int}]^2 \left[\frac{\tau}{1+\omega^2\tau^2} \right] \operatorname{sech}^2(E/2K_BT). \tag{12}$$

In (12), $H_{\rm int}$ is the hyperfine field (averaged over the different sites), γ is the nuclear gyromagnetic ratio, τ is the rare-earth relaxation time, and $\omega/2\pi$ is the resonance frequency. E is the exchange energy splitting of the rare-earth ion and the sech^2 term becomes zero when the lower Kramers doublet becomes fully populated. The dimensionless factor F determines the amount of transverse hyperfine field and will be different for different sites. For the case when $\vec{M}_{Fe}$ is along ⟨111⟩ or ⟨100⟩ the factors F can be written in rather simple forms[17]:

For $\vec{M}_{Fe}$ along ⟨100⟩,

$$F(c_1) = 0, \tag{13a}$$

$$F(c_2) = \tfrac{1}{8} \frac{(f_x^2 - f_y^2)^2}{(f_x^2 + f_y^2)} ; \tag{13b}$$

for $\vec{M}_{Fe}$ along ⟨111⟩,

$$F(c_1') = \tfrac{1}{6} \frac{(f_x^2 - f_z^2)^2}{(f_z^2 + 2f_x^2)} \tag{14a}$$

$$F(c_2') = \tfrac{1}{6} \frac{(f_y^2 - f_z^2)^2}{(f_z^2 + 2f_y^2)} . \tag{14b}$$

In (13) and (14) the parameters f_x characterize the anisotropic hyperfine interaction. The parameter $f_x = \nu_x/\bar{\nu}$, etc., where ν_x, ν_y, and ν_z are the principal values of ν along the orthorhombic axes.

TABLE III. Values of T_1 obtained for the various sites with an applied field of about 5 kG.

Orientation	Site	H_{ext} (kG)	T_1 (msec)
⟨100⟩	c_1	4.5	2.8 – 6
	c_2	4.5	≈5
⟨111⟩	c_1' or c_2'	5.6	≈1.0
	c_2' or c_1'	4.5	≈0.05

We have used (12) to evaluate T_1 for the different sites. In evaluating the quantities F we have taken $\nu_z = 690$ MHz, $\nu_x = 400$ MHz, and $\nu_y = 300$ MHz.

The Er^{+3} relaxation time τ in Er-substituted YIG has been found[19] to be 10^{-11} sec at 55 °K. At 4.2 °K it can be estimated to be about 3×10^{-11} sec. Assuming τ to have the same value in ErIG would give $\omega\tau \ll 1$. It has been assumed that τ has the same value for the different sites.

The relaxation times are particularly sensitive to the exchange splittings E. We have taken for E an average value[20] of 25 cm^{-1} which we assume to be the same for each site. While this is not correct it should at least provide an order of magnitude estimate of T_1. With these assumptions T_1 differs for each site only through the factor F. For site c_1, F is zero and so there is no contribution to T_1 from this mechanism. For site c_2 we obtain $T_1 = 0.44$ msec, while for the two ⟨111⟩ sites we obtain T_1's of 0.06 and 0.03 msec. Consequently, there appears to be at least rough order-of-magnitude agreement between the calculated T_1's and the experimental values of Table III. More precise values of E are needed for a better test of theory and experiment.

Besides the direct relaxation mechanism just discussed there should be an indirect one in which the rare-earth nuclei is relaxed by rare-earth ions on neighboring sites. Such a mechanism should be important for site c_1, for which the direct mechanism should not be effective. The indirect relaxation mechanism would be field dependent as in the case of the Fe^{57} indirect relaxation and this may explain the dependence of T_1 on field shown in Fig. 4.

Finally we will briefly consider the transverse relaxation. As a consequence of the quadrupole splitting, T_2 will be much less than T_1. According to Walstedt[21] we expect the transverse relaxation to be exponential with a T_2 contribution which is related to T_1 by the expression $T_1/T_2' = (I+\frac{1}{2})^2$. This factor is 16 for a spin-$\frac{7}{2}$ system. We find that the factors $T_1/16T_2$ vary between about 0.3 and 5 for the different sites, indicating that there may be in some cases an additional contribution to T_2 other than the Walstedt contribution. Such an additional contribution to T_2 could arise from indirect nuclear-spin–spin interactions.

VI. CONCLUSION

From both the static and dynamic NMR studies we have been able to derive detailed information about the rare-earth ions in ErIG which we have correlated with results of other studies. The over-all agreement between theory and experiment appears to be rather good as far as the static NMR studies are concerned. In the case of the relaxation time studies lack of precise values of the rare-earth exchange splittings limit the accuracy with which the theoretical relaxation times can be calculated but rough agreement between theory and experiment is obtained.

[1] F. W. Harrison, J. F. A. Thompson, and G. K. Lang, J. Appl. Phys. **36**, 1014 (1965).
[2] E. Orlich and S. Hüfner, Z. Phys. **232**, 418 (1970).
[3] R. L. Streever and P. J. Caplan, Phys. Lett. A 33, 412 (1970).
[4] S. Hüfner, P. Keinle, W. Weidermann, S. Frey, and W. Zinn, in *Proceedings of the International Conference on Magnetism, Nottingham, 1964* (The Institute of Physics and the Physical Society, London, 1965), p. 672.
[5] R. J. Elliott and K. W. H. Stevens, Proc. R. Soc. A 218, 553 (1953).
[6] R. J. Elliott, Rev. Mod. Phys. **30**, 385 (1964).
[7] W. P. Wolf, M. Ball, M. T. Hutchings, M. J. M. Leask, and A. F. J. Wyatt, J. Phys. Soc. Jap. Suppl. **17**, 443 (1962).
[8] R. L. Streever and P. J. Caplan, Phys. Rev. B 3, 2910 (1971).
[9] E. Belorizky, Y. Ayant, D. Descamps, and Y. M. D'Aubigne, J. Phys. (Paris) **27**, 133 (1966).
[10] R. L. Cohen and J. H. Wernick, Phys. Rev. **134**, B503 (1964).
[11] Le Dang Khoi, J. Phys. (Paris) Suppl. **32**, C1–1146 (1971).
[12] A. J. Freeman and R. E. Watson, Phys. Rev. **127**, 2058 (1962).
[13] P. Grünberg, S. Hüfner, E. Orlich, and J. Schmitt, Phys. Rev. **184**, 285 (1969).
[14] W. W. Simmons, W. J. O'Sullivan, and W. A. Robinson, Phys. Rev. **127**, 1168 (1962).
[15] A. Narath, Phys. Rev. **162**, 320 (1967).
[16] F. Hartmann-Boutron, Phys. Kondens. Mater. **2**, ,(1964).
[17] S. M. Myers, H. Myer, and J. P. Remeika, J. Phys. Chem. Solids **32**, 867 (1971).
[18] J. H. Van Vleck and R. Orbach, Phys. Rev. Lett. **11**, 65 (1963).
[19] B. H. Clarke, R. F. Pearson, R. W. Teale, and K. Tweedale, J. Appl. Phys. **34**, 1269 (1963).
[20] J. R. Dean, D. Bloor, G. M. Copland, and V. Sells, AIP Conf. Proc. **5**, 259 (1972).
[21] R. E. Walstedt, Phys. Rev. Lett. **19**, 146 (1967); Phys. Rev. Lett. **19**, 816 (1967).